Magnetic behavior near the boundary of 4f delocalization in ferromagnetic $CeRu_2Ge_2$ and paramagnetic $CeRu_2Si_2$ observed by Ce $M_{4,5}$ XAS and XMCD

T. Okane,[1,*] Y. Takeda,[1] H. Yamagami,[1,2] A. Fujimori,[1,3] Y. Matsumoto,[4,†] N. Kimura,[4] T. Komatsubara,[4] and H. Aoki[4]

[1]*Quantum Beam Science Directorate, Japan Atomic Energy Agency, Hyogo 679-5148, Japan*

[2]*Department of Physics, Kyoto Sangyo University, Kyoto 603-8555, Japan*

[3]*Department of Physics, University of Tokyo, Tokyo 113-0033, Japan*

[4]*Graduate School of Science and Center for Low Temperature Science, Tohoku University, Miyagi 980-8578, Japan*

(Received 26 April 2012; published 27 September 2012)

X-ray absorption (XAS) and its magnetic circular dichroism (XMCD) were measured at the Ce $M_{4,5}$ absorption edges of ferromagnetic $CeRu_2Ge_2$ and paramagnetic $CeRu_2Si_2$: both compounds are considered to be located near the boundary of delocalization of Ce 4f electrons. While the XAS line shape varies clearly reflecting the variation in the 4f delocalization, the line-shape variation in XMCD is hardly discernible under various conditions of temperature and magnetic field. The XAS line-shape variation can be explained as effects of the variations in the 4f occupation number and in the ratio of $J = 7/2$ states in the ground states, both of which are closely related to the 4f delocalization. The 4f delocalization also causes a decrease in the ratio of the orbital magnetic moment to the spin magnetic moment. The magnetic-field dependence of XAS suggests that the Ce 4f electrons retain a delocalized character across the metamagnetic transition in $CeRu_2Si_2$.

DOI: 10.1103/PhysRevB.86.125138 PACS number(s): 71.27.+a, 75.20.Hr, 75.30.Kz, 75.30.Mb

I. INTRODUCTION

The physical properties of cerium compounds are widely variable by controlling temperature, external field, pressure, stoichiometry, and so on, and they are summarized as the Doniach phase diagram,[1,2] as shown in Fig. 1. The Doniach phase diagram assumes that the competing relation between the Ruderman-Kittel-Kasuya-Yosida (RKKY) interaction and the Kondo effect is described as a function of $J_{cf}D(\varepsilon_F)$, where J_{cf} denotes the magnitude of magnetic exchange interaction and $D(\varepsilon_F)$ is the electronic density of states at the Fermi level ε_F. In the small $J_{cf}D(\varepsilon_F)$ region, the Ce 4f electrons have a localized nature and magnetic order is realized below the magnetic transition temperature (T_{mag} in Fig. 1). As $J_{cf}D(\varepsilon_F)$ increases, the Kondo effect is overcoming the RKKY interaction, thus suppressing the magnetic order, and the Ce 4f electrons form an itinerant heavy fermion state. The disappearance of magnetic order defines a quantum critical point (QCP) with a possible delocalization of Ce 4f electrons and an unconventional superconductivity is often found in the vicinity of QCP.[3]

The $CeRu_2(Ge_{1-x}Si_x)_2$ system, where the Si atoms are substituted for the Ge atoms of $CeRu_2Ge_2$ with the tetragonal $ThCr_2Si_2$ structure, is a good example of the system describable within the Doniach phase diagram. $CeRu_2Ge_2$ shows a ferromagnetic order below the Curie temperature $T_C \approx 7.5$ K.[4,5] The Ce 4f electrons of $CeRu_2Ge_2$ are considered to be localized, because the Fermi surfaces obtained from the de Haas–van Alphen (dHvA) and angle-resolved photoelectron spectroscopy (ARPES) experiments[6–8] are consistent with the theoretically obtained Fermi surfaces including no 4f electrons.[9] The magnetic order turns from ferromagnetic to antiferromagnetic with the substitution of the Si atoms for the Ge atoms, i.e., increase of x in $CeRu_2(Ge_{1-x}Si_x)_2$, and it vanishes above the critical composition $x_c \approx 0.93$.[10–12] The substitution is interpreted as a chemical pressure. In $CeRu_2Si_2$, the Ce 4f electrons are considered to form a heavy fermion state below the Kondo temperature T_K of 20–25 K with a large value of specific heat coefficient $\gamma \approx 350$ mJ/(mol K^2).[13–15] The itinerant nature of the Ce 4f electrons below T_K is suggested from a comparison of the Fermi surfaces between the experimental (dHvA and ARPES) and the theoretical results.[16–24] On the other hand, $CeRu_2Si_2$ shows a metamagnetic transition above the critical field $H_M \approx 7.7$ T along the [001] direction,[25,26] indicating that $CeRu_2Si_2$ is located near the boundary of an emergence of magnetic order or the boundary of 4f localization.

In comparison between $CeRu_2Ge_2$ and $CeRu_2Si_2$, it is an important issue to clarify what kind of differences in the Ce 4f electronic states bring about the emergence or the absence of magnetic order in the ground state. X-ray magnetic circular dichroism (XMCD) reveals the magnetic polarization effect on a certain electron orbital of a specific element in a compound as a variation in the line shape of x-ray-absorption (XAS) spectra measured at the selected absorption edges, and hence is a useful experimental technique to investigate the relationship between magnetism and electronic states. The information about the magnetism of Ce 4f electrons is obtained from the XMCD spectra measured at the Ce $M_{4,5}$ ($3d \rightarrow 4f$) absorption edges. Authors of the previous experimental works of Ce $M_{4,5}$ XMCD reported that a difference in the line shape of the XMCD spectra was observed on several Ce compounds.[27,28] In these works, the difference in the XMCD line shape was attributed to the different strength of hybridization between Ce 4f and conduction electrons (c-f hybridization). Since the increase of the c-f hybridization should enhance the delocalization of Ce 4f electrons, the line shape of Ce $M_{4,5}$ XMCD may be different between $CeRu_2Ge_2$ and $CeRu_2Si_2$.

In this work, we have measured the Ce $M_{4,5}$ XMCD of ferromagnetic $CeRu_2Ge_2$ below T_C and paramagnetic $CeRu_2Si_2$ below T_K in order to clarify the difference of the XAS and the XMCD spectra between the 4f-localized and the 4f-delocalized states. Another important issue for $CeRu_2Si_2$ is whether the Ce 4f electrons are localized or not at the

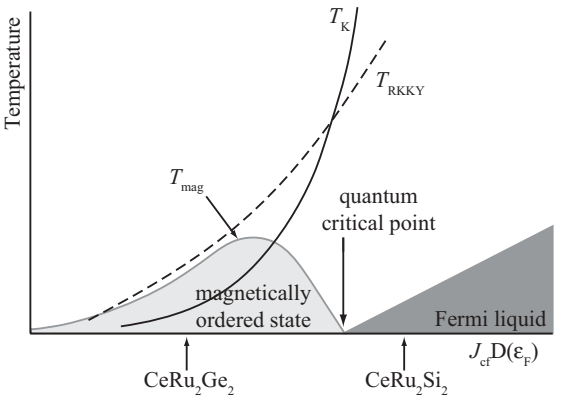

FIG. 1. Typical Doniach phase diagram. T_{RKKY} and T_K denote characteristic temperatures of RKKY interaction and Kondo effect, respectively. T_{mag} indicates a magnetic ordering temperature.

high-field state above the critical field $H_M \approx 7.7$ T of the metamagnetic transition.[11,12,16–18] Therefore we carried out a comparison of the XAS and the XMCD spectra below and above H_M. Also we investigated the temperature dependence of the line shape of the XAS and the XMCD spectra, since it is also a general issue whether the itinerant Ce $4f$ electrons in the heavy fermion state become localized at high temperatures above the Kondo temperature T_K.[1] The application of the sum rule[29,30] to the Ce $M_{4,5}$ XMCD, which was once doubted on the validity of the spin sum rule by the previous Ce $M_{4,5}$ XMCD experiments,[27] is carefully examined for the data of $CeRu_2Ge_2$ and $CeRu_2Si_2$.

II. EXPERIMENT

The samples of $CeRu_2Ge_2$ and $CeRu_2Si_2$ were single crystals grown by the Czokralski pulling method in a tetra-arc furnace under high-purity argon gas atmosphere. They were annealed for a week at 900 °C under vacuum. Details of the sample preparation are described in Ref. 12.

The XMCD measurements at the Ce $M_{4,5}$ edges were performed at the beamline BL23SU of SPring-8.[31,32] In the XMCD measurements, a magnetic field up to 10 T, produced by a superconducting magnet, was applied to the sample along the [001] direction, which is an easy axis of magnetization, while circularly polarized x rays irradiated the sample along the same direction. A combination of the operations of both the monochromator and the twin helical undulator brings about a helicity switching of circular polarization by 1 Hz at each energy.[33] XAS spectra were obtained by the total electron yield method. XMCD signals were obtained by reversing the helicity of x rays under the fixed direction of the magnetic field, or by reversing the direction of the magnetic field under the fixed x-ray helicity. The samples were cooled by a liquid-helium cryostat and the temperature was controlled in the range between 4.6 and 250 K.

III. RESULTS

A. XMCD and magnetic field dependence

Figure 2 presents the Ce $M_{4,5}$ XAS and XMCD spectra of $CeRu_2Ge_2$ in the ferromagnetic state and of $CeRu_2Si_2$ in the paramagnetic state. The XAS spectra measured with the helicity of circularly polarized x rays parallel and antiparallel to the direction of the magnetization are denoted by "+ helicity" and "− helicity," respectively. The XMCD spectra were obtained as a difference of the XAS spectra measured with + and − helicities. The magnitude of the XMCD signal is larger in $CeRu_2Ge_2$ than in $CeRu_2Si_2$, reflecting the magnitude of the magnetic moment of the Ce $4f$ electrons. As seen in Fig. 2, the line shapes of the XAS and the XMCD spectra are almost identical to the results in the previous works.[19,27,28,34]

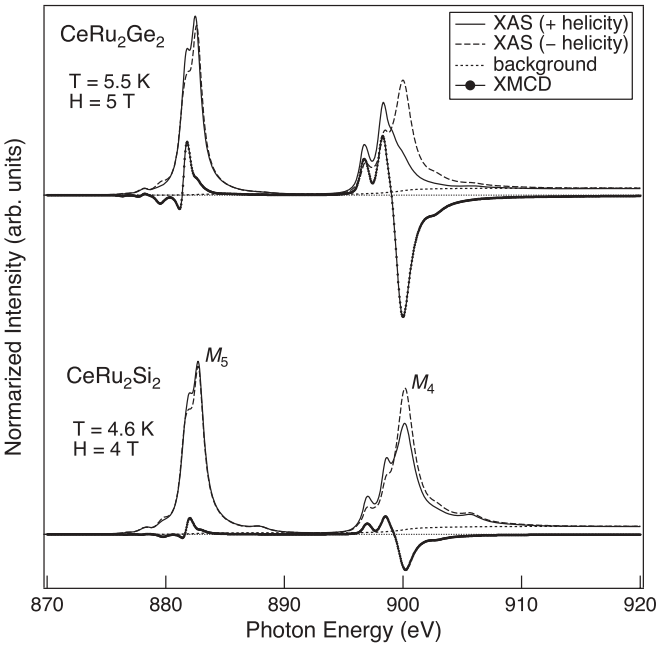

FIG. 2. XAS and XMCD spectra at the Ce $M_{4,5}$ edges of $CeRu_2Ge_2$ and $CeRu_2Si_2$. The spectra of $CeRu_2Ge_2$ were measured at the sample temperature of 5.5 K under the magnetic field of 5 T in the ferromagnetic state, and the spectra of $CeRu_2Si_2$ were measured at 4.6 K under 4 T in the paramagnetic state. Each of the spectra has been normalized to the unity at the M_5 peak of the XAS spectrum. Backgrounds of the XAS spectra were assumed to be an integral type as indicated in the figure.

Figure 3 demonstrates the magnetic field dependencies of the intensity of the dominant XMCD peak at the M_4 edge of $CeRu_2Ge_2$ and $CeRu_2Si_2$. The data of $CeRu_2Ge_2$ at 5.5 K indicates a clear ferromagnetic transition, while a paramagnetic linear dependence is observed at 20 K. A metamagnetic transition at $H_M \approx 7.7$ T is unclear in the data of $CeRu_2Si_2$ at 4.6 K, since clear transition would be observed at the temperature below 2 K.[25] However, the difference between 4.6 and 10 K demonstrates that a trace of the metamagnetic transition appears as a slight hump at around 7.7 T, and thus the metamagnetic transition can be tracked even at the temperature of 4.6 K. The upturn of the difference in the range 0–4 T is understood as a temperature dependence of Brillouin function.

B. Comparison of line shape

Fine structures in the Ce $M_{4,5}$ XAS spectra are understood as multiplet structures of the final states of the absorption process from the $4f^1$ and $4f^0$ configurations in the initial

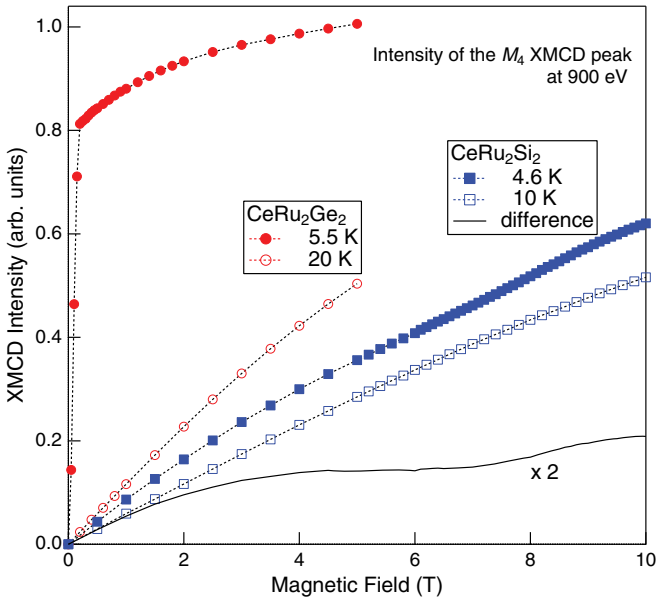

FIG. 3. (Color online) Magnetic field dependencies of the intensity of the dominant M_4 XMCD peak at 900 eV. Red closed and open circles with dotted lines denote the data of $CeRu_2Ge_2$ measured below T_C (5.5 K) and above T_C (20 K). Blue closed and open squares with dotted lines denote the data of $CeRu_2Si_2$ measured at 4.6 and at 10 K, respectively. Solid curve indicates the difference between 4.6 and 10 K.

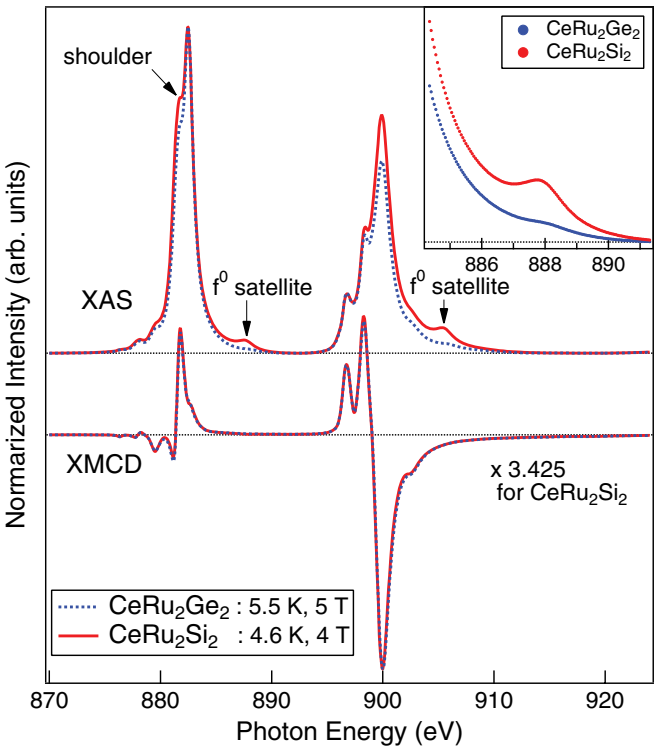

FIG. 4. (Color online) Ce $M_{4,5}$ XAS and XMCD spectra of ferromagnetic $CeRu_2Ge_2$ (blue broken line) and paramagnetic $CeRu_2Si_2$ (red solid line). Conditions on temperature and magnetic field are the same as in Fig. 2. Integral-type backgrounds in Fig. 2 have been subtracted for the XAS spectra in Figs. 4–6. The intensities of the XAS and the XMCD spectra have been normalized to the intensity of the dominant XAS peak at the M_5 edge, while the intensity of the XMCD spectrum of $CeRu_2Si_2$ has been multiplied by 3.425. The inset presents a magnified view of the f^0 satellite at the M_5 edge.

state, while the contribution of the $4f^2$ initial configuration is negligibly small.[35–37] Both in the M_5 and the M_4 XAS spectra, satellite structures originated from the $4f^0$ configuration in the ground state, which will be referred to as "f^0 satellite" hereafter, appear at the higher energy side of the leading XAS peak.[35] It is generally considered that, as the f^0 satellite becomes stronger, the number of Ce $4f$ electrons decreases from 1.0, indicating that the Ce $4f$ electrons becomes more delocalized due to an increase of the c-f hybridization.

On the other hand, the line shape of the Ce $M_{4,5}$ XMCD spectra is understood as multiplet structures arising almost only from the $4f^1$ configuration in the ground state, since the $4f^0$ configuration does not contribute to the magnetism. From the atomic multiplet calculation,[36] a variation of the XMCD line shape appears as the mixing ratio between the $J = 5/2$ and $J = 7/2$ states of the $4f^1$ configuration, depending on the c-f hybridization strength.[28,37] Since different degrees of $4f$ delocalization due to the different strengths of the c-f hybridization are possibly realized in the states between (1) ferromagnetic $CeRu_2Ge_2$ and paramagnetic $CeRu_2Si_2$, (2) below and above the critical field H_M of the metamagnetic transition of $CeRu_2Si_2$, and (3) below and above the Kondo temperature T_K of $CeRu_2Si_2$, we have examined differences of the Ce $M_{4,5}$ XAS and XMCD line shapes for the above-mentioned three comparisons.

1. *Ferromagnetic $CeRu_2Ge_2$ and paramagnetic $CeRu_2Si_2$*

Figure 4 demonstrates a comparison of line shapes of the Ce $M_{4,5}$ XAS and XMCD spectra between ferromagnetic $CeRu_2Ge_2$ and paramagnetic $CeRu_2Si_2$. The XAS spectra were obtained as a half of the sum of the XAS spectra measured with + and − helicities. The intensities have been adjusted so that the dominant M_5 peak coincides in the XAS spectra and the dominant negative M_4 peak coincides in the XMCD spectra between $CeRu_2Ge_2$ and $CeRu_2Si_2$ for the sake of the comparison of the line shapes.

Comparing the XAS line shapes, the f^0 satellite structures are clearly observed both at the M_5 and the M_4 edges of $CeRu_2Si_2$, while the f^0 satellite is negligibly small in $CeRu_2Ge_2$ even in the magnified view of the f^0 satellite region shown in the inset of Fig. 4. The results indicate that the occupation number of the Ce $4f$ electrons slightly decreases from 1.0 in $CeRu_2Si_2$, while the $4f$ occupation number nearly equals 1.0 in $CeRu_2Ge_2$. The results are consistent with the previously suggested picture that the Ce $4f$ electrons form an itinerant heavy fermion state in $CeRu_2Si_2$, while the Ce $4f$ electrons of $CeRu_2Ge_2$ are almost localized.

Another noticeable difference in the XAS line shape between $CeRu_2Ge_2$ and $CeRu_2Si_2$ is that the branching ratio $B_R = I(M_5)/[I(M_5) + I(M_4)]$, where $I(M_5)$ and $I(M_4)$ denote the integrated XAS intensities at the M_5 and the M_4 absorption edges, respectively, decreases from $CeRu_2Ge_2$ to $CeRu_2Si_2$. The estimated B_R values are 0.518 and 0.489 for $CeRu_2Ge_2$ and $CeRu_2Si_2$, respectively. It is noteworthy that these estimated B_R values are substantially larger than the theoretically obtained maximum B_R value of 0.46 for the Ce^{3+}

ion obtained by the atomic calculation.[35] The other difference in the XAS line shape is that the shoulder structure, which is located at the lower energy side of the leading M_5 XAS peak, is stronger in $CeRu_2Si_2$ than in $CeRu_2Ge_2$.

In contrast, the XMCD line shapes of $CeRu_2Ge_2$ and $CeRu_2Si_2$ are almost identical and overlap with each other, contrary to our expectation. An important point here is that the intensity ratio between the M_4 and the M_5 components of the XMCD spectra is almost the same between $CeRu_2Ge_2$ and $CeRu_2Si_2$, even though the M_4:M_5 intensity ratio is remarkably different in the XAS spectra. In addition, the difference in the intensity of the shoulder structure of the M_5 XAS spectra does not bring about a difference in the XMCD line shape. On the other hand, it is reasonable that the difference of the strength of the f^0 satellite produces no effect in the XMCD spectra, because the f^0 configuration in the initial states should not contribute to the magnetism.

2. *$CeRu_2Si_2$ below and above H_M*

If the Ce $4f$ electrons of $CeRu_2Si_2$ above H_M of the metamagnetic transition were localized as in ferromagnetic $CeRu_2Ge_2$, the line shapes of the Ce $M_{4,5}$ XAS and XMCD spectra would be changed. However, the $4f$ electron nature is considered to be continuous around the metamagnetic transition, and is rapidly smeared out with a slight increase of temperature even below 4 K.[10,38,39] Therefore our measurement temperature of 4.6 K is insufficient to observe a clear change of the $4f$ electron nature around the metamagnetic transition. Nevertheless, the metamagnetic transition at $H_M \approx$ 7.7 T was traced in the magnetic field dependence of the XMCD intensity, as shown in Fig. 3.

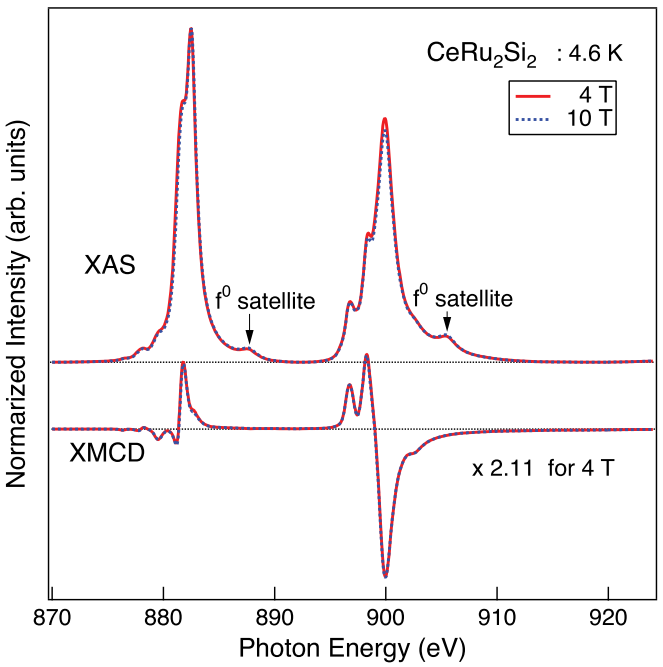

FIG. 5. (Color online) Ce $M_{4,5}$ XAS and XMCD spectra of $CeRu_2Si_2$ measured at 4.6 K under the magnetic field of 4 T (red solid line) and 10 T (blue broken line). The intensities of XAS and the XMCD spectra have been normalized to the intensity of dominant XAS peak at the M_5 edge, while the intensity of the XMCD spectrum at 4 T has been multiplied by 2.11.

Figure 5 presents a comparison of the Ce $M_{4,5}$ XAS and XMCD spectra of $CeRu_2Si_2$ measured under the magnetic field below H_M (4 T) and above H_M (10 T). The intensities of the spectra presented here are adjusted in the same way as used in Fig. 4. Invariance of the f^0 satellite indicates that the $4f$ occupation number is unchanged along the metamagnetic transition and remains to be deviated from unity even above H_M. On the other hand, one can see that the peak top at the M_4 edge is slightly lower at 10 T than at 4 T. This brings about a slight increase of B_R from 0.489 at 4 T to 0.493 at 10 T. The XMCD line shape shows no noticeable changes along the metamagnetic transition.

3. *Temperature dependence*

In heavy fermion Ce compounds, it is often suggested that Ce $4f$ electrons, which are itinerant below T_K, are possibly localized at temperatures above T_K, since the high-temperature behavior of the magnetic susceptibility is explained by the Curie-Weiss-type behavior of the Ce^{3+} ion. Figure 6 shows a comparison of the Ce $M_{4,5}$ XAS and XMCD spectra of $CeRu_2Si_2$ and measured at the temperature of 4.6 K, which is below $T_K \approx 20$ K, and at 150 and 250 K far above T_K. The Ce $M_{4,5}$ XAS and XMCD spectra of $CeRu_2Ge_2$ at 5.5 K, which is below T_C, and 250 K are also shown in the figure. All the spectra here were measured under magnetic fields that are sufficient to establish the magnetic orders at low temperatures. The intensities of the spectra have been adjusted in the same way as used in Fig. 4.

Interestingly, while the XAS line shapes of $CeRu_2Si_2$ measured at 4.6 and 150 K almost coincide with each other, the intensity of the f^0 satellite structure clearly decreases at 250 K. For the XAS spectra of $CeRu_2Ge_2$, the peak top at the M_4 edge is higher in 250 K than in 5.5 K, indicating a slight decrease of B_R from 0.518 at 5.5 K to 0.509 at 250 K. These variations in the XAS line shape shall be discussed in Sec. IV B.

In the comparison of the XMCD spectra, a clear temperature variation in the line shape has not been observed in both $CeRu_2Si_2$ and $CeRu_2Ge_2$, taking into account the poorer S/N ratio of the XMCD signals measured at 250 K. Combined with the results in Secs. III B1 and III B2, it is concluded that the Ce $M_{4,5}$ XMCD line shape is less sensitive to the small variation in electronic structures than the Ce $M_{4,5}$ XAS line shape.

IV. ANALYSIS AND DISCUSSION

A. Sum-rule analysis

One can quantitatively estimate the values of the orbital magnetic moment μ_L and the spin magnetic moment μ_S of Ce $4f$ electrons by applying the orbital and spin sum rules,[29,30]

$$\frac{\langle L_z \rangle}{3n_h} = \frac{\int_{M_4+M_5} \Delta\gamma(E)dE}{\frac{3}{2}\int_{M_4+M_5} \gamma(E)dE}, \quad (1)$$

$$\frac{2}{3}\frac{\langle S_z \rangle + 3\langle T_z \rangle}{n_h} = \frac{\int_{M_5} \Delta\gamma(E)dE - \frac{3}{2}\int_{M_4} \Delta\gamma(E)dE}{\frac{3}{2}\int_{M_4+M_5} \gamma(E)dE}, \quad (2)$$

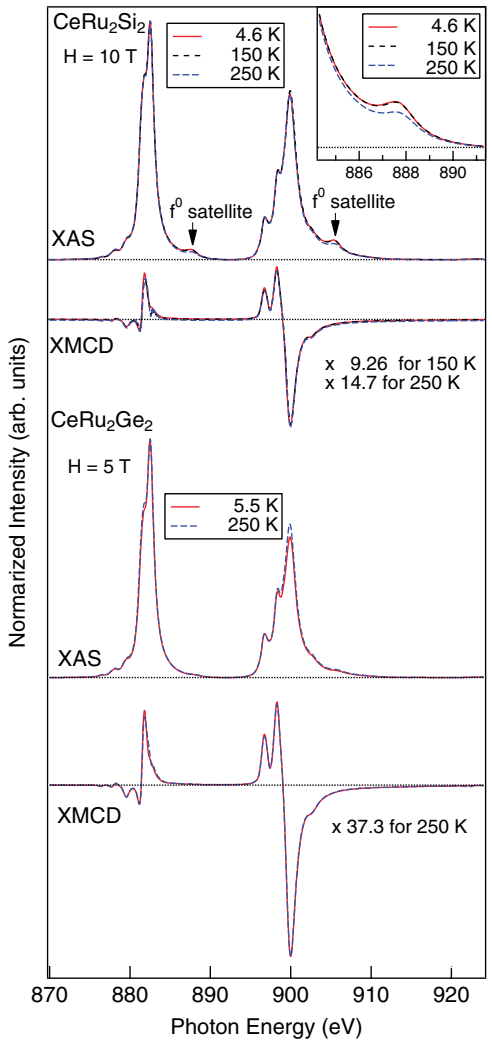

FIG. 6. (Color online) Ce $M_{4,5}$ XAS and XMCD spectra of $CeRu_2Si_2$ measured at 4.6 K (red solid line), 150 K (dotted line), and 250 K (blue broken line) under the magnetic field of 10 T, and of $CeRu_2Ge_2$ measured at 5.5 K (red solid line) and 250 K (blue broken line) under 5 T. The intensities of XAS and the XMCD spectra have been normalized to the intensity of the dominant XAS peak at the M_5 edge, while the intensities have been multiplied by 9.26 and 14.7 for the XMCD spectra of $CeRu_2Si_2$ at 150 and 250 K, respectively, and by 37.3 for the XMCD spectra of $CeRu_2Ge_2$ at 250 K. The inset shows a magnified view of the f^0 satellite at the M_5 edge.

to the integrated intensities of Ce $M_{4,5}$ XAS and XMCD spectra. Here, $\langle L_z\rangle$, $\langle S_z\rangle$, and $\langle T_z\rangle$ are the expectation values with respect to the z component of the orbital angular momentum, the spin angular momentum, and the magnetic dipole operator of the 4f shell, respectively. $\gamma(E)$ represents the energy dependence of XAS spectrum, which is equal to $[\gamma_+(E)+\gamma_-(E)]/2$, where $\gamma_+(E)$ and $\gamma_-(E)$ denote XAS spectra measured with a circular polarization of $+$ and $-$ helicities, respectively. Then, $\Delta\gamma(E)$, which is equal to $\gamma_+(E)-\gamma_-(E)$, describes the energy dependence of XMCD spectrum. n_h is the number of holes in the 4f shell, and will be assumed to be 13.0 in the calculation hereafter, since the 4f occupation number is close to 1.0 both in $CeRu_2Ge_2$ and $CeRu_2Si_2$. Then, one can estimate the orbital and spin

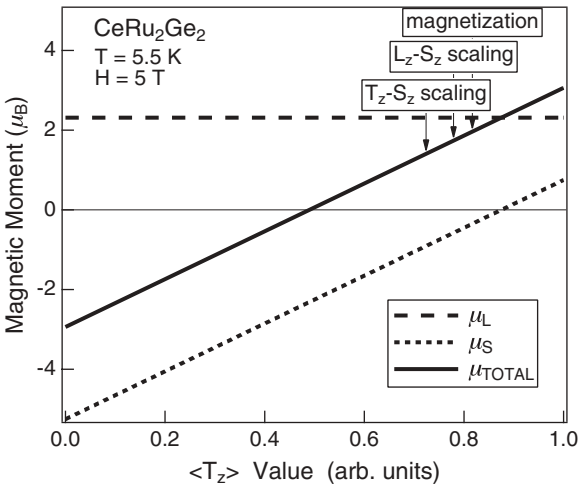

FIG. 7. $\langle T_z\rangle$ dependencies of the orbital magnetic moment μ_L (broken line), the spin magnetic moment μ_S (dotted line), and the total magnetic moment μ_{TOTAL} (solid line) of Ce 4f electrons estimated from the application of the sum rule to the integrated intensity of the XAS and XMCD spectra of $CeRu_2Ge_2$ measure at 5.5 K under the magnetic field of 5 T.

magnetic moments of Ce 4f electrons as $\mu_L=-\langle L_z\rangle\mu_B$, $\mu_S=-2\langle S_z\rangle\mu_B$, and the total magnetic moment as $\mu_{TOT}=\mu_L+\mu_S$.

In the previous Ce $M_{4,5}$ XMCD work,[27] it was suggested that the spin sum rule of Eq. (2) is invalid for Ce $M_{4,5}$ XMCD and cannot be used to deduce the spin contribution to the 4f moment, while the orbital sum rule of Eq. (1) is applicable still. The reason for the disability of the spin sum rule would be imposed from the fact that Coulomb interaction mixes spin-orbit-split states for the case of Ce $M_{4,5}$ absorption edges, since the energy separation between the M_5 and the M_4 edges induced from the spin-orbit parameter is not sufficiently large compared to the Slater integrals.[35–37] On the other hand, in the case of the magnetism of electrons which possess more or less a localized nature, the magnitude of $\langle T_z\rangle$, which cannot be experimentally determined, is expected to be comparable to that of $\langle S_z\rangle$. Therefore different ways of estimation of $\langle T_z\rangle$ result in a wide variation in the estimated value of μ_S.

Figure 7 demonstrates the $\langle T_z\rangle$ dependencies of the values of μ_L, μ_S, and μ_{TOTAL} evaluated from the application of Eqs. (1) and (2) to the integrated intensities of the Ce $M_{4,5}$ XAS and XMCD spectra of $CeRu_2Ge_2$ in the ferromagnetic states (5.5 K, 5 T). The magnetization value[5] of $\approx 1.96\mu_B$ at 4.2 K under 5 T is indicated by an arrow inscribed as "magnetization" in Fig. 7 for comparison. One can notice from the $\langle T_z\rangle$ dependencies of the estimated magnetic moments that the assumption of $\langle T_z\rangle=0$ brings about a serious overestimation of μ_S, resulting in the wrong sign of μ_{TOTAL}. Therefore the assumption of negligible $\langle T_z\rangle$, which is frequently used in the case of $L_{2,3}$ XMCD for 3d transition-metal compounds, is inappropriate in the case of Ce $M_{4,5}$ XMCD.

Another way to evaluate μ_L, μ_S, and μ_{TOTAL} from the Ce $M_{4,5}$ XAS and XMCD spectra without the spin sum rule is as follows. Assuming that $\langle S_z\rangle$ is scaled with $\langle L_z\rangle$ and the ratio $\langle L_z\rangle/\langle S_z\rangle$ in the Hund's rule states is applicable, μ_S is evaluated from the μ_L value estimated from the orbital sum

rule of Eq. (1) and the ratio $\langle L_z\rangle/\langle S_z\rangle$. The assumption is not going too far, since the magnetic behavior of $CeRu_2Ge_2$ and $CeRu_2Si_2$ are described by the Hund's rule $4f^1\ ^2F_{5/2}$ states as discussed in Sec. IV B. The ratio $\langle L_z\rangle/\langle S_z\rangle$ in the $4f^1\ ^2F_{5/2}$ states is equal to -8, resulting in $\mu_L/\mu_S = -4$. Thus the spin component is obtained as $\mu_S = -\mu_L/4$. The value of $\mu_{TOT} = \mu_L + \mu_S$ evaluated in this method is indicated by an arrow inscribed as "$\langle L_z\rangle$-$\langle S_z\rangle$ scaling" in Fig. 7. Although the sum rule analysis in the $\langle L_z\rangle$-$\langle S_z\rangle$ scaling provides the μ_{TOTAL} value close to the magnetization value, the assumption of the fixed ratio of μ_L/μ_S seems to be unreasonable for the case when the degree of $4f$ delocalization is different. To put it in the other way, we cannot discuss the degree of $4f$ delocalization from the analysis of the XMCD spectra using the $\langle L_z\rangle$-$\langle S_z\rangle$ scaling.

Therefore we adopt the third way to evaluate the magnetic moments, which uses the spin sum rule as follows. By assuming that $\langle T_z\rangle$ is scaled with $\langle S_z\rangle$, we can eliminate the $\langle T_z\rangle$ term from Eq. (2). The ratio $\langle T_z\rangle/\langle S_z\rangle$ is calculated using the theoretical expectation values of $\langle T_z\rangle$ and $\langle S_z\rangle$ for the Hund's rule states.[40] Using Eq. (17) and the values of Table VI in Ref. 40, the expectation values of $\langle T_z\rangle$ and $\langle S_z\rangle$ are calculated as $\langle T_z\rangle = -\langle w^{211}\rangle/3 = 4/7$ and $\langle S_z\rangle = -\langle w^{011}\rangle/2 = 5/14$, resulting in $\langle T_z\rangle/\langle S_z\rangle = 8/5$. Using the value of $\langle T_z\rangle/\langle S_z\rangle$, the $\langle T_z\rangle$ term in Eq. (2) is eliminated and thus μ_S will be evaluated using Eq. (2). The value of μ_{TOT} evaluated in this method is indicated by an arrow inscribed as "$\langle T_z\rangle$-$\langle S_z\rangle$ scaling" in Fig. 7. The μ_{TOTAL} values estimated from the sum rule analysis in the $\langle T_z\rangle$-$\langle S_z\rangle$ scaling are close to the magnetization value, although somewhat underestimated. The discrepancy with the magnetization value may arise from the underestimation of μ_L in the sum-rule analysis, or the contribution from the magnetic polarization of conduction electrons, which may be included in the magnetization data. The comparatively good μ_{TOTAL} value obtained in the $\langle T_z\rangle$-$\langle S_z\rangle$ scaling implies that an appropriate scaling of the $\langle T_z\rangle$ enables us to estimate μ_S from the application of the spin sum rule to Ce $M_{4,5}$ XMCD.

Table I summarizes the values of μ_L, μ_S, μ_{TOT}, and the ratio μ_L/μ_S of Ce $4f$ electrons of the Ce $M_{4,5}$ XAS and XMCD spectra of $CeRu_2Ge_2$ and $CeRu_2Si_2$ under several conditions of temperature and magnetic field, estimated from the sum-rule analysis. From the estimated values in the $\langle T_z\rangle$-$\langle S_z\rangle$ scaling, one can investigate the tendency of the variation in the $|\mu_L/\mu_S|$ value, which might be closely related to the variation in the c-f hybridization strength. Table I indicates that the $|\mu_L/\mu_S|$ value decreases when the system is changed from ferromagnetic $CeRu_2Ge_2$ (5.5 K, 5 T) to paramagnetic $CeRu_2Si_2$ (4.6 K, 4 T), from the above-H_M state (4.6 K, 10 T) to the below-H_M state (4.6 K, 4 T) in $CeRu_2Si_2$, from the high-temperature state above T_K (250 K, 10 T) to the low-temperature state below T_K (4.6 K, 10 T) in $CeRu_2Si_2$ above H_M. Since the Ce $4f$ electrons are expected to become more delocalized in the above three cases, the decrease of $|\mu_L/\mu_S|$ can be considered as an index of the $4f$ delocalization.

B. Discussion

As mentioned in Sec. III B1, the primary characteristics in the line-shape variation of the Ce $M_{4,5}$ XAS spectra from ferromagnetic $CeRu_2Ge_2$ (5.5 K, 5 T) to paramagnetic $CeRu_2Si_2$ (4.6 K, 4 T) are (1) the decrease of the branching ratio B_R, (2) the enhancement of the f^0 satellite structure, and (3) the enhancement of the M_5 shoulder structure. In order to evaluate the variation in the line shapes of the Ce $M_{4,5}$ XAS and XMCD spectra between ferromagnetic $CeRu_2Ge_2$ (5.5 K, 5 T) and paramagnetic $CeRu_2Si_2$ (4.6 K, 4 T) quantitatively, we have performed a line-shape analysis demonstrated in Fig. 8 as an example for $CeRu_2Si_2$. Details of the analysis is described in the Appendix. It shows that the decrease of B_R is mainly caused by the marked increase in the intensity of the M_4 leading peak [component r in Fig. 8(c)], while the intensities of the other components [components p and q in Fig. 8(c)] in the triple structures are almost unchanged. The intensity ratio of the f^0 satellite structure increases from ~2% of the total $M_{4,5}$ XAS intensity in $CeRu_2Ge_2$ (5.5 K, 5 T) to ~6% in $CeRu_2Si_2$ (4.6 K, 4 T), and the intensity of the M_5 shoulder structure of $CeRu_2Si_2$ increases as ~118% of that of $CeRu_2Ge_2$. In the comparison of the XMCD line shapes under the fixed M_4 XMCD intensity, the noticeable variation is observed only in the sum of the leading negative and positive components [components E and F in Fig. 8(b)] at the M_5 edge, resulting in a variation in the intensity ratio M_5/M_4 from -0.23 of $CeRu_2Ge_2$ to -0.26 of $CeRu_2Si_2$. From the equations of the sum rules, one can see that a variation in the intensity ratio of the orbital to the spin magnetic moments μ_L/μ_S is roughly connected with the ratio M_5/M_4 of the XMCD spectra. Thus the slight increase of the leading M_5 XMCD components produces a considerable decrease in the ratio $|\mu_L/\mu_S|$ estimated from the sum-rule analysis of the XMCD spectra in Sec. IV A in spite of the almost unchanged XMCD line shape.

The line shapes of the XAS and XMCD spectra at the Ce $M_{4,5}$ edges are expected to be different depending on the degree of $4f$ delocalization. Besides the f^0 satellite structure in the XAS spectra, one possible idea to explain the line-shape variation in the XAS and XMCD spectra is that a variation in the mixing ratio of $J = 5/2$ states to $J = 7/2$ states of the $4f^1$ configuration in the ground states might bring about different

TABLE I. Values of the orbital magnetic moment μ_L, the spin magnetic moment μ_S, the total magnetic moment μ_{TOT}, and the ratio μ_L/μ_S of Ce $4f$ electrons of $CeRu_2Ge_2$ and $CeRu_2Si_2$ in units of μ_B, estimated from the sum-rule analysis of the Ce $M_{4,5}$ XMCD data.

		$\langle L_z\rangle$-$\langle S_z\rangle$ scaling				$\langle T_z\rangle$-$\langle S_z\rangle$ scaling			
		μ_L	μ_S	μ_{TOT}	μ_L/μ_S	μ_L	μ_S	μ_{TOT}	μ_L/μ_S
$CeRu_2Ge_2$	5.5 K, 5 T	2.312	−0.578	1.734	−4.0	2.312	−0.905	1.407	−2.55
	250 K, 5 T	0.057	−0.014	0.043	−4.0	0.057	−0.023	0.034	−2.50
$CeRu_2Si_2$	4.6 K, 4 T	0.511	−0.128	0.383	−4.0	0.511	−0.215	0.296	−2.38
	4.6 K, 10 T	1.200	−0.300	1.000	−4.0	1.200	−0.470	0.730	−2.55
	250 K, 10 T	0.089	−0.022	0.067	−4.0	0.089	−0.032	0.057	−2.77

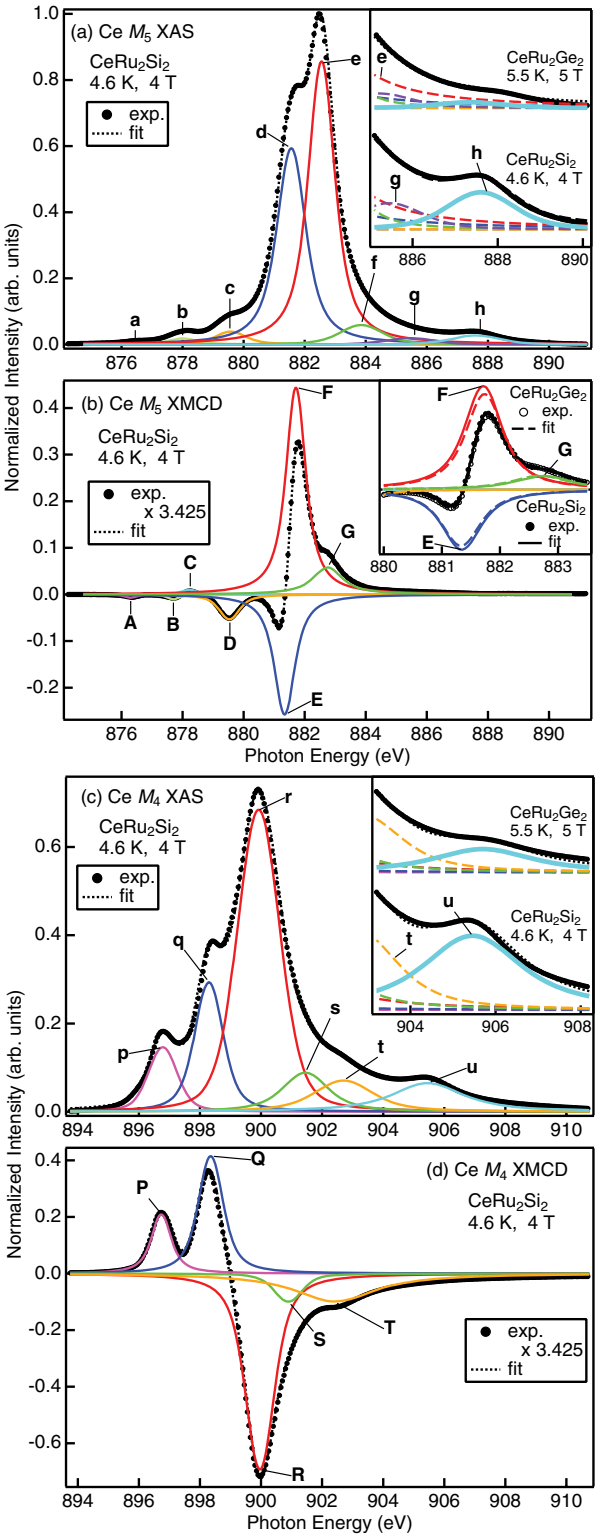

FIG. 8. (Color online) Line-shape analysis of the Ce M_5 XAS (a), the Ce M_5 XMCD (b), the Ce M_4 XAS (c), and the Ce M_4 XMCD (d) spectra of $CeRu_2Si_2$ at 4.6 K under 4 T. The intensity of the XMCD spectrum has been multiplied by 3.425. The insets in (a) and (c) illustrate a comparison of the f^0 satellite structures between $CeRu_2Si_2$ (4.6 K, 4 T) and $CeRu_2Ge_2$ (5.5 K, 5 T) in a magnified view. The inset in (b) illustrates a comparison of the M_5 XMCD line shape between $CeRu_2Si_2$ (4.6 K, 4 T) and $CeRu_2Ge_2$ (5.5 K, 5 T) in a magnified view.

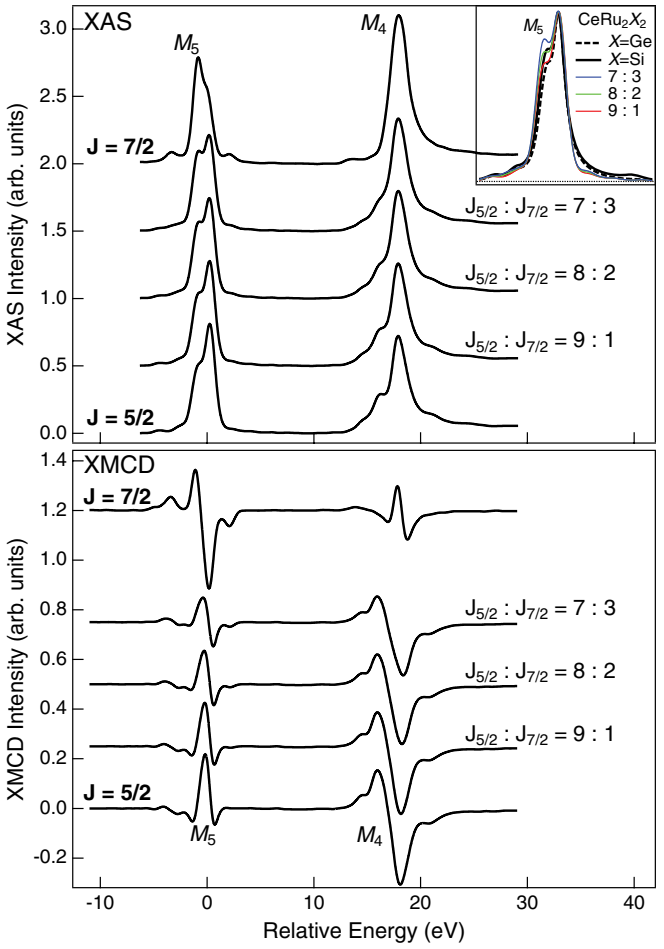

FIG. 9. (Color online) XAS and XMCD spectra at the Ce $M_{4,5}$ edges calculated for $J = 5/2$ and $J = 7/2$ states of Ce $4f^1$ configuration, referred from Fig. 2 of Ref. 28. In addition, the weighted sums of the $J = 5/2$ and $J = 7/2$ components in the ratio $J_{5/2}$:$J_{7/2}$ of 7:3, 8:2, and 9:1 are illustrated. The inset illustrates a comparison of the M_5 XAS spectra between the calculation and the experimental data of $CeRu_2Ge_2$ (5.5 K, 5 T) and $CeRu_2Si_2$ (4.6 K, 4 T).

line shapes. It was theoretically predicted that the weight of $J = 7/2$ states relative to $J = 5/2$ states increases with the c-f hybridization strength, and the amount of the $J = 7/2$ character in the ground states becomes considerable when the hybridization strength Δ is of the order of the energy necessary to excite an electron from $J = 5/2$ states to above the Fermi level ($N^{1/2}\Delta \geqslant \varepsilon_f$, where ε_f is the energy of the $f^1_{5/2}$ level with the degeneracy N).[37,41] The atomic multiplet calculation of the $3d^{10}4f^1|JM\rangle \rightarrow 3d^9 4f^2|J'M'\rangle$ transition[36] predicted that the theoretical line shapes of the Ce $M_{4,5}$ XAS and XMCD spectra are significantly different between $J = 5/2$ and $J = 7/2$ states,[28] as shown in Fig. 9. Using these calculated line shapes, we demonstrate a line-shape variation of the $M_{4,5}$ XAS and XMCD spectra as a weighted sum of the line shapes for $J = 5/2$ and $J = 7/2$ states, also shown in Fig. 9.

One can see from Fig. 9 that, as the weight of $J = 7/2$ in the ground state increases, the M_4 XAS peak becomes stronger relative to the M_5 peak, resulting in the decrease of B_R, and the shoulder structure in the M_5 XAS spectra is more enhanced. In

the free-atom case, the branching ratio has a maximum for the Hund's-rule ground state of $J = 5/2$ and its value gradually decreases with J.[42–44] The B_R variation originated from the $J = 7/2$ mixing ratio is consistent with the line-shape analysis that only the leading peak [component r in Fig. 8(c)] among the triple peak structures in the M_4 XAS spectra contributes to the variation in B_R. Therefore the variations from ferromagnetic $CeRu_2Ge_2$ (5.5 K, 5 T) to paramagnetic $CeRu_2Si_2$ (4.6 K, 4 T) can be interpreted as an increase of the $J = 7/2$ weight in the ground states caused by the increase in the c-f hybridization strength. The tendency is consistent with the variation of the f^0 intensity. The inset to Fig. 9 shows that the variation from ferromagnetic $CeRu_2Ge_2$ and paramagnetic $CeRu_2Si_2$ roughly corresponds to 10% increase of $J = 7/2$ states.

The experimentally obtained Ce $M_{4,5}$ XMCD spectra is basically explained by the calculated line shape for the $J = 5/2$ state. The line-shape variation in Fig. 9 demonstrates that the relative intensity of the M_5 signal slightly decreases as the $J = 7/2$ weight increases, while the overall line shape of the $M_{4,5}$ XMCD spectra is similar within the small ratio of $J = 7/2$ states less than 30%. It is indicated from the line-shape analysis that the intensity ratio $|M_5/M_4|$ in the XMCD spectra slightly increases from ferromagnetic $CeRu_2Ge_2$ (5.5 K, 5 T) to paramagnetic $CeRu_2Si_2$ (4.6 K, 4 T). The observed $|M_5/M_4|$ tendency is contradictory to an increase of the $J = 7/2$ weight, which is expected from the $M_{4,5}$ XAS line shape. Therefore the variation observed in the XMCD spectra cannot be explained by the scenario of the increase in the $J = 7/2$ weight. The inconsistency might be related to the discrepancy in the M_5 XMCD line shape between experiment and calculation: while the calculation indicates the existence of the negative peak at the higher energy side of the dominant positive peak, the experiment shows a positive shoulder structure [component G in Fig. 8(b)] at that part. Therefore we need an improved theoretical treatment of the line-shape variation of the Ce $M_{4,5}$ XMCD spectra, while a more pronounced variation in the XMCD line shape should be examined in future XMCD experiments for Ce compounds with high T_K.

dHvA experiments revealed that the Fermi surfaces of $CeRu_2Si_2$ above the critical field H_M of the metamagnetic transition resemble the Fermi surfaces of $LaRu_2Si_2$, while the experimental Fermi surfaces below H_M are explained by the calculated Fermi surfaces of $CeRu_2Si_2$.[16–18,23,24] Since Ce compounds with localized $4f$ electrons are expected to have Fermi surfaces of La compounds, there is a possibility that the $4f$ electrons of $CeRu_2Si_2$ turns from delocalized one to localized one at H_M. This is contrary to the observation that the f^0 intensity in the XAS spectra of $CeRu_2Si_2$ is unchanged across the metamagnetic transition. However, the metamagnetic transition in $CeRu_2Si_2$ is a crossover type, where the localization of the $4f$ electrons may proceed gradually and continuously across the transition.[11,12,39] There, the $4f$ electron states, which are located at the Fermi level E_F in the paramagnetic states, may become separated from E_F, downward for the up-spin band and upward for the down-spin band, in the ferromagnetic states above H_M due to the Zeeman shift.[45,46] In this situation, Fermi surfaces become similar to those of $LaRu_2Si_2$ because the $4f$ electron states are located at the positions away from E_F and less hybridized with conduction bands.[47,48] However, the $4f$ electrons should still possess a considerable amount of itinerant character because the c-f hybridized bands are preserved in the states above H_M. As a result, the $4f$ occupation number may not be significantly changed across the metamagnetic transition as observed in our XAS data. Although our result suggests that the $4f$ electrons of $CeRu_2Si_2$ are still delocalized above H_M of the metamagnetic transition, it is an interesting subject in the future how the f^0 satellite intensity will change in the measurement below 2 K, where the metamagnetic transition becomes sharper.

The temperature-dependent decrease in the f^0 satellite intensity in the XAS spectra of $CeRu_2Si_2$, which is directly related to the decrease in the $4f$ occupation number, was observed surprisingly not across T_K but in the temperature region ten times larger than T_K, i.e., between 150 and 250 K. Therefore the temperature-dependent decrease in the $4f$ occupation number cannot be simply explained by the localization of the Ce $4f$ electrons. Another possible explanation is crystal-field effect, since the crystal-field splitting of $CeRu_2Si_2$ between the ground-state doublet and the next doublet was estimated to be 220 K from the specific-heat measurement.[15] Since crystal-field splitting in Kondo systems arises from an anisotropy in the mixing interaction,[49] the crystal-field excited state would have a different $4f$ occupation number due to different c-f hybridization strength.

The branching ratio B_R of the XAS spectra tends to decrease from the ferromagnetic state to the paramagnetic state, as shown in the following cases: from ferromagnetic $CeRu_2Ge_2$ to paramagnetic $CeRu_2Si_2$, from the above-H_M state to the below-H_M state in $CeRu_2Si_2$, and from the below-T_C state to the above-T_C state in $CeRu_2Ge_2$. Since B_R is considered to be an index of c-f hybridization strength, the result suggests that magnetic ordering might be related to the variation in the c-f hybridization.

V. CONCLUSIONS

We have measured XAS and XMCD spectra at the Ce $M_{4,5}$ edges of $CeRu_2Ge_2$ and $CeRu_2Si_2$ under several conditions of temperature and magnetic field, in order to clarify the difference of the magnetic properties of the Ce $4f$ electrons near the boundary of $4f$ delocalization. Comparing paramagnetic $CeRu_2Si_2$ with ferromagnetic $CeRu_2Ge_2$, delocalization of the Ce $4f$ electrons was verified in the Ce $M_{4,5}$ XAS spectra as a growth of the f^0 satellite structures from ~2% to ~6% of the total $M_{4,5}$ XAS intensity, a decrease in the branching ratio $B_R = I(M_5)/[I(M_5) + I(M_4)]$ from 0.52 to 0.49, and an enhancement of the M_5 XMCD shoulder structure to become ~118% of $CeRu_2Ge_2$. Those variations in the XAS line shape can be explained by the idea of the increase in the c-f hybridization strength, resulting in the decrease of the $4f$ occupation number and the increase of the ratio of $J = 7/2$ states relative to $J = 5/2$ states in the ground state. Although the overall line shape of the Ce $M_{4,5}$ XMCD spectra is scarcely changed, a slight increase in the intensity ratio $|M_5/M_4|$ of the XMCD spectra results in the decrease of the ratio of the orbital to the spin magnetic moments $|\mu_L/\mu_S|$, which corresponds to the $4f$ delocalization. It is suggested from the invariance of the f^0 satellite intensity in the XAS spectra that the Ce $4f$ electrons of $CeRu_2Si_2$ in the state just above the critical field of the metamagnetic transition retain an itinerant character. The

temperature-dependent decrease of the 4f occupation number in $CeRu_2Si_2$ is attributed to crystal-field effect. Future XMCD study for the Ce compounds with high T_K would reveal more clearly the hybridization-dependent variation in the XMCD line shape.

ACKNOWLEDGMENTS

We are very grateful to Y. Saitoh for his great efforts in improving the XMCD measurement system of BL23SU at SPring-8. We also thank A. Kotani and A. Tanaka for helpful discussions on the theoretical treatment of the Ce $M_{4,5}$ XMCD spectra. This work was performed under Proposals No. 2009B3823, No. 2010A3823, and No. 2011A3835 in BL23SU at SPring-8, and is supported by Grant-in-Aid for Scientific Research Grants No. 20102003 and No. 23540430 from the Ministry of Education, Culture, Sports, Science and Technology, Japan.

APPENDIX: LINE-SHAPE ANALYSIS

The line-shape analysis demonstrated in Fig. 8 was performed under the following ideas. Fixed values of Lorentzian and Gaussian broadenings for each component were used in common, and energy positions of each component are slightly adjusted. Only the relative intensities of each component were markedly changed between $CeRu_2Ge_2$ and $CeRu_2Si_2$. Here, the intensities of the experimentally obtained XAS and XMCD spectra to be fitted were normalized in the same way as in Fig. 4 in order to estimate the line-shape variation as a relative ratio among each component. The fitting parameters deduced from the analysis are summarized in Table II.

TABLE II. Values of fitted parameters, i.e., Lorentzian half width at half maximum (HWHM), and Gaussian HWHM, energy position, and intensity, used in the line-shape analysis of the Ce $M_{4,5}$ XAS and XMCD spectra of $CeRu_2Ge_2$ at 5.5 K under 5 T and $CeRu_2Si_2$ at 4.6 K under 4 T, demonstrated in Figs. 8(a)–8(d).

M_5 XAS	a	b	c	d	e	f	g	h
Lorentzian HWHM (eV)	0.30	0.38	0.38	0.40	0.38	0.38	0.38	0.38
Gaussian HWHM (eV)	0.01	0.30	0.35	0.30	0.27	0.38	0.70	0.72
Energy position (eV)								
$CeRu_2Ge_2$ (5.5 K, 5 T)	876.40	877.95	879.55	881.57	882.56	883.70	885.20	887.35
$CeRu_2Si_2$ (4.6 K, 4 T)	876.45	878.00	879.57	881.56	882.55	883.85	885.45	887.60
Intensity (arb. units)								
$CeRu_2Ge_2$ (5.5 K, 5 T)	0.003	0.024	0.050	0.805	1.310	0.100	0.025	0.010
$CeRu_2Si_2$ (4.6 K, 4 T)	0.003	0.028	0.064	0.950	1.280	0.125	0.045	0.065
M_5 XMCD	A	B	C	D	E	F	G	
Lorentzian HWHM (eV)	0.20	0.20	0.20	0.30	0.35	0.33	0.55	
Gaussian HWHM (eV)	0.10	0.10	0.15	0.20	0.15	0.15	0.15	
Energy position (eV)								
$CeRu_2Ge_2$ (5.5 K, 5 T)	876.33	877.73	878.23	879.54	881.33	881.74	882.69	
$CeRu_2Si_2$ (4.6 K, 4 T)	876.30	877.70	878.23	879.53	881.34	881.71	882.75	
Intensity (arb. units)								
$CeRu_2Ge_2$ (5.5 K, 5 T)	−0.005	−0.0075	0.0083	−0.062	−0.295	0.477	0.108	
$CeRu_2Si_2$ (4.6 K, 4 T) × 3.425	−0.005	−0.0075	0.0083	−0.062	−0.315	0.517	0.105	
M_4 XAS	p	q	r	s	t	u		
Lorentzian HWHM (eV)	0.19	0.26	0.23	0.60	0.70	1.20		
Gaussian HWHM (eV)	0.45	0.40	0.69	0.50	0.70	0.50		
Energy position (eV)								
$CeRu_2Ge_2$ (5.5 K, 5 T)	896.77	898.30	899.92	901.50	902.80	905.70		
$CeRu_2Si_2$ (4.6 K, 4 T)	896.78	898.29	899.92	901.45	902.70	905.45		
Intensity (arb. units)								
$CeRu_2Ge_2$ (5.5 K, 5 T)	0.213	0.410	1.085	0.160	0.160	0.085		
$CeRu_2Si_2$ (4.6 K, 4 T)	0.200	0.420	1.340	0.220	0.220	0.270		
M_4 XMCD	P	Q	R	S	T			
Lorentzian HWHM (eV)	0.30	0.30	0.35	0.25	1.60			
Gaussian HWHM (eV)	0.18	0.30	0.35	0.40	0.10			
Energy position (eV)								
$CeRu_2Ge_2$ (5.5 K, 5 T)	896.74	898.36	900.00	900.95	902.44			
$CeRu_2Si_2$ (4.6 K, 4 T)	896.73	898.35	899.96	900.89	902.42			
Intensity (arb. units)								
$CeRu_2Ge_2$ (5.5 K, 5 T)	0.235	0.535	−1.080	−0.150	−0.515			
$CeRu_2Si_2$ (4.6 K, 4 T) × 3.425	0.235	0.555	−1.080	−0.140	−0.500			

At the Ce M_5 edge, components for the shoulder structure, the leading peak, and the f^0 satellite structure in the XAS spectra are d, e, and h, respectively. A major contribution in the M_5 XMCD spectra is produced from the counterbalance between the negative component E and the positive component F. The energy positions of both E and F in the M_5 XMCD spectra are close to the positions of the shoulder structure d rather than the leading peak e in the M_5 XAS spectra. Therefore the major contribution in the M_5 XMCD is attributed to the shoulder structure in the M_5 XAS spectra, while the leading peak in the M_5 XAS spectra seems to be responsible for the component G in the M_5 XMCD spectra. The energy positions of A, B, and D in the M_5 XMCD spectra correspond to the positions of a, b, and c in the M_5 XAS spectra, respectively. There is no XMCD structure at the energy position corresponding to f, g, and h in the M_5 XAS spectra.

At the Ce M_4 edge, the triple peak structures in the XAS spectra are attributed to the components p, q, and r. The fitting component for the f^0 satellite is u. The small hump in between the leading XAS peak and the f^0 satellite can be realized by introducing additional components s and t. The energy positions of two positive peaks, P and Q, and one negative dominant peak, R, in the M_4 XMCD spectra agree well with the positions of p, q, and r in the M_4 XAS spectra. The energy position of the component T in the M_5 XMCD spectra corresponds to the positions of s and t in the M_4 XAS spectra.

The increase in the intensity of the component r, where the value for $CeRu_2Si_2$ (4.6 K, 4 T) is ~123.5% of the value for $CeRu_2Ge_2$ (5.5 K, 5 T), is responsible for the decrease of B_R from $CeRu_2Ge_2$ to $CeRu_2Si_2$. In $CeRu_2Si_2$ (4.6 K, 4 T), the intensity ratio of the f^0 satellite structure h at the M_5 edge is ~2.5% of the entire M_5 XAS intensity, while the intensity ratio of the f^0 satellite structure u at the M_4 edge is ~10% of the entire M_4 XAS intensity. The intensity ratio of h + u is ~6% of the total $M_{4,5}$ XAS intensity. In $CeRu_2Ge_2$ (5.5 K, 5 T), the intensity ratio of h is ~0.4% of the M_5 XAS intensity, while that of u is ~4% of the M_4 XAS intensity. The intensity ratio of h + u is ~2% of the $M_{4,5}$ XAS intensity. The intensity ratio of the f^0 satellite structure is clearly larger in the M_4 edge than in the M_5 edge, although that might be influenced by the broadening widths used in the fitting. The intensity of the M_5 shoulder structure d is clearly stronger in $CeRu_2Si_2$ (4.6 K, 4 T) than in $CeRu_2Ge_2$ (5.5 K, 5 T): the value of $CeRu_2Si_2$ is ~118% of that of $CeRu_2Ge_2$.

The comparison of the XMCD line shapes shows that the intensities of the components A, B, C, and D at the M_5 edge and the components P, Q, R, S, and T at the M_4 edge are almost the same between ferromagnetic $CeRu_2Ge_2$ (5.5 K, 5 T) and paramagnetic $CeRu_2Si_2$ (4.6 K, 4 T). Only the components E and F, which produce the dominant M_5 XMCD structure as a mixture of negative and positive contributions, show notable increases in the magnitudes from $CeRu_2Ge_2$ to $CeRu_2Si_2$. Although this variation in the relatively small signal of the M_5 spectra is hardly discernible and therefore the overall XMCD line shape seems almost unchanged in appearance, it brings about a significant variation as a ratio M_5/M_4.

The variations depending on magnetic field in $CeRu_2Si_2$ (Sec. III B2) and temperature in $CeRu_2Si_2$ and $CeRu_2Ge_2$ (Sec. III B3) can be explained in the same line. In the comparison between $CeRu_2Si_2$ (4.6 K, 10 T) and $CeRu_2Si_2$ (250 K, 10 T) as a temperature dependence, the intensities of the f^0 satellite structures h and u at the M_5 and the M_4 edges of $CeRu_2Si_2$ (250 K, 10 T) decrease as ~69% and ~80% of those of $CeRu_2Si_2$ (4.6 K, 10 T), respectively.

*okanet@spring8.or.jp
†Present address: Advanced Science Research Center, Japan Atomic Energy Agency, Ibaraki 319-1195, Japan.

[1] Y. Ōnuki, R. Settai, K. Sugiyama, T. Takeuchi, T. C. Kobayashi, Y. Haga, and E. Yamamoto, J. Phys. Soc. Jpn. **73**, 769 (2004).
[2] S. Doniach, *Valence Instabilities and Related Narrow Band Phenomena*, edited by R. D. Parks (Plenum, New York, 1977), p. 169.
[3] P. Gegenwart, Q. Si, and F. Steglich, Nat. Phys. **4**, 186 (2008).
[4] A. Böhm, R. Caspary, U. Habel, L. Pawlak, and A. Zuber, F. Steglich, and A. Loidl, J. Magn. Magn. Mater. **76-77**, 150 (1988).
[5] M. J. Besnus, A. Essaihi, N. Hamdaoui, G. Fischer, J. P. Kappler, A. Meyer, J. Pierre, P. Haen, and P. Lejay, Physica B **171**, 350 (1991).
[6] C. A. King and G. G. Lonzarich, Physica B **171**, 161 (1991).
[7] H. Ikezawa, H. Aoki, M. Takashita, C. J. Haworth, S. Uji, T. Terahsima, K. Maezawa, R. Settai, and Y. Onuki, Physica B **237-238**, 210 (1997).
[8] M. Yano, A. Sekiyama, H. Fujiwara, T. Saita, S. Imada, and T. Muro, Y. Ōnuki, and S. Suga, Phys. Rev. Lett. **98**, 036405 (2007).
[9] H. Yamagami and A. Hasegawa, J. Phys. Soc. Jpn. **63**, 2290 (1992).
[10] P. Haen, H. Bioud, and T. Fukuhara, Physica B **259-261**, 85 (1999).
[11] M. Sugi, Y. Matsumoto, N. Kimura, T. Komatsubara, H. Aoki, T. Terashima, and S. Uji, Phys. Rev. Lett. **101**, 056401 (2008).
[12] Y. Matsumoto, M. Sugi, K. Aoki, Y. Shimizu, N. Kimura, T. Komatsubara, H. Aoki, M. Kimata, T. Terashima, and S. Uji, J. Phys. Soc. Jpn. **80**, 074715 (2011).
[13] A. Loidl, G. Knopp, H. Spille, F. Steglich, and A. P. Murani, Physica B **156-157**, 794 (1989).
[14] R. A. Fisher, C. Marcenat, N. E. Phillips, P. Haen, F. Lapierre, P. Lejay, J. Flouquet, and J. Voiron, J. Low Temp. Phys. **84**, 49 (1991).
[15] M. J. Besnus, J. P. Kappler. P. Lemann, and A. Meyer, Solid State Commun. **55**, 779 (1985).
[16] H. Aoki, S. Uji, A. K. Albessard, and Y. Ōnuki, Phys. Rev. Lett. **71**, 2110 (1993).
[17] H. Aoki, S. Uji, A. K. Albessard, and Y. Ōnuki, J. Phys. Soc. Jpn. **62**, 3157 (1993).
[18] M. Takashita, H. Aoki, T. Terashima, S. Uji, K. Maezawa, R. Settai, and Y. Ōnuki, J. Phys. Soc. Jpn. **65**, 515 (1996).
[19] M. Yano, A. Sekiyama, H. Fujiwara, Y. Amano, S. Imada, T. Muro, M. Yabashi, K. Tamasaku, A. Higashiya, and T. Ishikawa, Y. Ōnuki, and S. Suga, Phys. Rev. B **77**, 035118 (2008).
[20] T. Okane, T. Ohkochi, Y. Takeda, S.-I. Fujimori, A. Yasui, Y. Saitoh, H. Yamagami, A. Fujimori, Y. Matsumoto, M. Sugi, N. Kimura, T. Komatsubara, and H. Aoki, Phys. Rev. Lett. **102**, 216401 (2009).
[21] T. Okane, T. Ohkochi, Y. Takeda, S.-I. Fujimori, A. Yasui, Y. Saitoh, H. Yamagami, A. Fujimori, Y. Matsumoto, M. Sugi, N. Kimura, T. Komatsubara, and H. Aoki, Phys. Status Solidi B **247**, 697 (2010).

[22]T. Okane, I. Kawasaki, A. Yasui, T. Ohkochi, Y. Takeda, S.-I. Fujimori, Y. Saitoh, H. Yamagami, A. Fujimori, Y. Matsumoto, N. Kimura, T. Komatsubara, and H. Aoki, J. Phys. Soc. Jpn. **80**, SA060 (2010).
[23]H. Yamagami and A. Hasegawa, J. Phys. Soc. Jpn. **62**, 592 (1993).
[24]H. Yamagami and A. Hasegawa, J. Phys. Soc. Jpn. **61**, 2388 (1992).
[25]P. Haen, J. Flouquet, F. Lapierre, P. Lejay, and G. Remenyi, J. Low Temp. Phys. **67**, 391 (1987).
[26]J. Flouquet, P. Haen, S. Raymond, D. Aoki, and G. Knebel, Physica B **319**, 251 (2002).
[27]J. Ph. Schillé, F. Bertran, M. Finazzi, Ch. Brouder, J. P. Kappler, and G. Krill, Phys. Rev. B **50**, 2985 (1994).
[28]M. Finazzi, F. M. F. de Groot, A.-M. Dias, B. Kierren, F. Bertran, Ph. Sainctavit, J.-P. Kappler, O. Schulte, W. Felsch, and G. Krill, Phys. Rev. Lett. **75**, 4654 (1995).
[29]B. T. Thole, P. Carra, F. Sette, and G. van der Laan, Phys. Rev. Lett. **68**, 1943 (1992).
[30]P. Carra, B. T. Thole, M. Altarelli, and X. Wang, Phys. Rev. Lett. **70**, 694 (1993).
[31]A. Yokoya, T. Sekiguchi, Y. Saitoh, T. Okane, T. Nakatani, T. Shimada, H. Kobayashi, M. Takao, Y. Teraoka, Y. Hayashi, S. Sasaki, Y. Miyahara, T. Harami, and T. A. Sasaki, J. Synchrotron Radiat. **5**, 10 (1998).
[32]Y. Saitoh, T. Nakatani, T. Matsushita, A. Agui, A. Yoshigoe, Y. Teraoka, and A. Yokoya, Nucl. Instrum. Methods Phys. Res., Sect. A **474**, 253 (2001).
[33]Y. Saitoh, Y. Fukuda, Y. Takeda, H. Yamagami, S. Takahashi, Y. Asano, T. Hara, K. Shirasawa, M. Takeuchi, T. Tanaka, and H. Kitamura, J. Synchrotron Radiat. **19**, 388 (2012).
[34]J. Rothman, C. Meyer, D. Givord, J. Vogel, M. Finazzi, FA. Fontaine, J.-P. Kappler, and N. B. Brookes, J. Magn. Magn. Mater. **198-199**, 276 (1999).
[35]B. T. Thole, G. van der Laan, J. C. Fuggle, G. A. Sawatzky, R. C. Karnatak, and J.-M. Esteva, Phys. Rev. B **32**, 5107 (1985).
[36]J. B. Goedkoop, B. T. Thole, G. van der Laan, G. A. Sawatzky, F. M. F. de Groot, and J. C. Fuggle, Phys. Rev. B **37**, 2086 (1988).
[37]G. van der Laan, B. T. Thole, G. A. Sawatzky, J. C. Fuggle, R. Karnatak, J.-M. Esteva, and B. Lengeler, J. Phys. C **19**, 817 (1986).
[38]R. Daou, C. Bergemann, and S. R. Julian, Phys. Rev. Lett. **96**, 026401 (2006).
[39]T. Sakakibara, T. Tayama, K. Matsuhira, H. Mitamura, H. Amitsuka, K. Maezawa, and Y. Ōnuki, Phys. Rev. B **51**, 12030 (1995).
[40]G. van der Laan and B. T. Thole, Phys. Rev. B **53**, 14458 (1996).
[41]T. Jo and S. Imada, J. Phys. Soc. Jpn. **59**, 1421 (1990).
[42]B. T. Thole and G. van der Laan, Phys. Rev. A **38**, 1943 (1988).
[43]B. T. Thole and G. van der Laan, Phys. Rev. B **38**, 3158 (1988).
[44]G. van der Laan and B. T. Thole, Phys. Rev. Lett. **60**, 1977 (1988).
[45]K. Miyake and H. Ikeda, J. Phys. Soc. Jpn. **75**, 033704 (2006).
[46]Y. Aoki, T. D. Matsuda, H. Sugawara, H. Sato, H. Ohkuni, R. Settai, Y. Ōnuki, E. Yamamoto, Y. Haga, A. V. Andreev, V. Sechovsky, L. Hacela, H. Ikeda, and K. Miyake, J. Magn. Magn. Mater. **177-181**, 271 (1998).
[47]Y. Matsumoto, M. Sugi, N. Kimura, T. Komatsubara, H. Aoki, I. Satoh, T. Terashima, and S. Uji, J. Phys. Soc. Jpn. **77**, 053703 (2008).
[48]M. Suzuki and H. Hariama, J. Phys. Soc. Jpn. **79**, 024705 (2010).
[49]P. M. Levy and S. Zhang, Phys. Rev. Lett. **62**, 78 (1989).